MRR
Jurnal Polimesin
Department of Mechanical Engineering
State Polytechnic of Lhokseumawe
http://e-jurnal.pnl.ac.id/polimesin
e-ISSN : 2549-1999 No. : 1 Month : February
p-ISSN : 1693-5462 Volume : 23 Year : 2025

Processing dates: received on 2024-09-25, reviewed on 2025-01-05, accepted on 2025-01-16, online availability on 2025-02-28

A Framework for surface profile optimization in sinker-EDM via response surface methodology

Rohman[1*], Muhamad Taufik Ulhakim[2], Sukarman[2], Danang Supriyanto[2]

[1]Department of Mechanical Engineering, School of Wastukancana Technology, Purwakarta 41151, Indonesia

[2]Department of Mechanical Engineering, University of Buana Perjuangan Karawang, Karawang 41361, Indonesia

*Corresponding author**:** rohman@wastukancana.ac.id

Abstract

Sinker Electrical Discharge Machining (SEDM) is a powerful technique used for shaping hard materials and creating complex designs. SEDM effectively machines hardened steel, titanium, and tungsten carbide, materials challenging for conventional methods. This study aims to identify the optimal surface profile (*Ra*) as a response variable in the SEDM process. This study utilized hardened SKD11 as the workpiece and graphite as the electrode, employing Response Surface Methodology (RSM) for optimization. The investigation focused on the pulse current, spark-on time, and gap voltage as the input parameters. The findings revealed that Sample 7 achieved the smoothest surface (at Ra = 10 µm), while Sample 13 had the roughest (at Ra = 20 µm). The analysis of these results determined the ideal conditions for the pulse current at level 1, spark-on time at level 3, and gap voltage at level 3, resulting in a surface profile of 10.2 microns. The successful application of RSM optimization in SEDM significantly contributes to the precision machining of alloy steels, which plays a crucial role in material-processing operations.

Keywords:

Sinker Electrical Discharge Machining, material removal rate, surface profile, response surface methodology, material forming

1. Introductions

Sinker Electrical Discharge Machining (SEDM) is a highly efficient technique for machining hard materials and creating complex profiles. Materials such as hardened steel, titanium, and tungsten carbide, which are difficult to machine using traditional methods, can be cut with high precision using SEDM[1-4]. High precision is achievable because the SEDM process does not require physical contact between the tool and workpiece, and it uses electrical discharges to remove material [5]. Owing to the absence of mechanical cutting forces, this method is particularly suitable for materials prone to distortion and cracking under physical stress. Moreover, SEDM excels in creating high-precision complex shapes, including sharp angles, deep cavities, and small holes, which are difficult to achieve using conventional techniques. This process also produces a smooth surface, which often eliminates the need for additional processing. Its capability to machine hard materials and form intricate profiles makes SEDM a preferred choice in industries that demand high precision, such as mold manufacturing, aerospace, and automotive [6]. By using electrodes shaped according to the desired profile, the shape can be accurately transferred to the workpiece, making SEDM an ideal solution for overcoming the limitations of traditional machining methods.

Although this study adopted a different approach, previous researchers have conducted several studies on SEDM. Aliakbari and Baseri [7] reported SEDM process parameters, including pulse current, pulse-on time, and electrode rotation. The response parameter focuses on the Material Removal Rate (MRR), surface roughness (*Ra*), electrode wear rate (EWR), and Overcut (OC). Their research employed a Taguchi experimental design with three levels of testing, using X210Cr12 (SPK) as the workpiece material and pure copper (99.9% Cu) as the electrode. The results showed that the current, pulse time, rotational speed, and electrode geometry significantly affected *the MRR*, *EWR*, and *Ra*. A subsequent study by Sultan et al. [8] used Response Surface Methodology (RSM) with similar parameters, pulse current, spark-on time, and peak current, while analyzing , *Ra*, and *EWR* as response variables. Using EN 353 steel as the workpiece and copper as the electrode, they identified the optimal MRR, Ra, and EWR values under specific parameter settings. Using a tungsten-copper electrode, Chandramouli investigated SEDM on 17-4 precipitation-hardening stainless steel (PH Steel), with parameters such as the peak current, spark-on time, pulse-off time, and tool life. His findings revealed that these parameters significantly influenced MRR and *Ra*. Świercz et al. [9] optimized SEDM using the Taguchi and RSM methods with heat-treated 1.2713 tool steel and a copper electrode, focusing on *MRR* and *Ra*. Saeedi et al. [10] explored the SEDM of steel using Deep Neural Networks (DNN) to analyze the surface profile produced by the SEDM process. Sumanto et al.[11] applied the Taguchi method to evaluate the effects of three input parameters on the surface roughness and overcut diameter using SKD11 as the workpiece material and graphite as the electrode. Khoerudin et al.[12] employed the Taguchi approach with a copper electrode to assess similar parameters.

Although considerable research has been conducted on non-conventional SEDM machining, further studies are necessary to optimize the SEDM process for SKD11 using Response Surface Methodology (RSM). SKD11 is commonly used in detailed drawing processes. Unlike previous studies, this study adopted an experimental approach with RSM, focusing on three key input parameters: pulse current, spark-on time, and gap voltage. SKD11 was used as the workpiece material, while graphite was selected as the electrode material owing to its higher cutting speed than copper. The gap voltage, which represents the voltage between the two electrodes, determines the total spark energy and controls the intermittent gap between them. The primary response variable in this study was the optimized surface roughness (*Ra*), with the primary objective of determining the optimal settings for all selected parameters.

2. Method

2.1. Material

Graphite was used as the electrode and SKD11 as the workpiece material. Graphite electrodes have a layered crystalline structure in which carbon atoms are arranged in parallel layers [13]. This unique structure endows graphite electrodes with exceptional conductivity [14]. SKD11 complies with JIS G4404 standards and is classified as a high-chromium alloy steel, primarily composed of carbon (1.40-1.60%), manganese (max 0.6%), silicon (max 0.4%), chromium (11.00-13.00%), molybdenum (0.80-1.20%), and vanadium (0.20-0.50%) [15]. A high Cr content enhances the corrosion and oxidation resistance, whereas carbon and vanadium significantly improve the hardness and wear resistance. Mechanically, SKD11 achieved a hardness level of HRC 58-62 after heat treatment, demonstrating excellent wear resistance and sufficient toughness to prevent cracking and

fracturing. This makes it ideal for applications in molds, cutting tools, and dies used in cold-working processes.

2.2. Heat treatment and machining process

The heat treatment was carried out in a Nabertherm™ furnace set at 850 °C according to the guidelines of JIS G4404, which recommend an annealed hardening temperature range of 830-880 °C[15]. Maintaining this temperature for 40 min allowed for uniform structural changes. It reduces the internal stresses, facilitating the desired microscopic structure and optimal mechanical properties specified in JIS G4404, achieving a Rockwell C Hardness (HRC) of 58-62. After the annealed hardening process, quenching uses carbon dioxide (CO_2) gas to accelerate cooling, maintain precise temperature control, and minimize the risk of distortion or cracking. It also prevents contamination and rust formation, enhancing the material's overall quality and the consistency of the results. Hardness measurements were performed using an AR936 Portable Hardness Tester [16]. Fig. 1 illustrates the annealing hardening process employed in this study.

2.3. Respond Surface Methodology

RSM was utilized to optimize the SEDM machining process by employing input parameters, such as the pulse current (A), gap voltage (V), and spark-on time (µs), to determine the optimal conditions for enhancing machining performance. RSM incorporates an experimental design to investigate variations among these three parameters and gather data on response variables, such as the surface profile and material removal rate (Fig. 2). The surface profile is linked to the surface quality, whereas the material removal rate is related to the production efficiency. Surface profile measurements were performed using an Elcometer™ 456, which provided a measurement accuracy of 0.1 microns. These measurements were conducted at room temperature, approximately 25-26 °C, within the recommended operational range of -10 to 50 °C. Fig. 3 illustrates the measurement of the workpiece surface profile resulting from the SEDM process.

Fig. 1. Surface profile measurements.

A multilinear regression approach was used as the response parameter to predict the influence of the three input variables on the surface profile. Statistical software was employed to derive the equation for predicting the surface profile, which was then compared and analyzed against the experimental data.

Fig. 2. Material Preparation of SKD11: (a) heat treatment process (JIS G 4404 standards), (b) hardness measurement prior to heat treatment, and (c) hardness measurement after heat treatment.

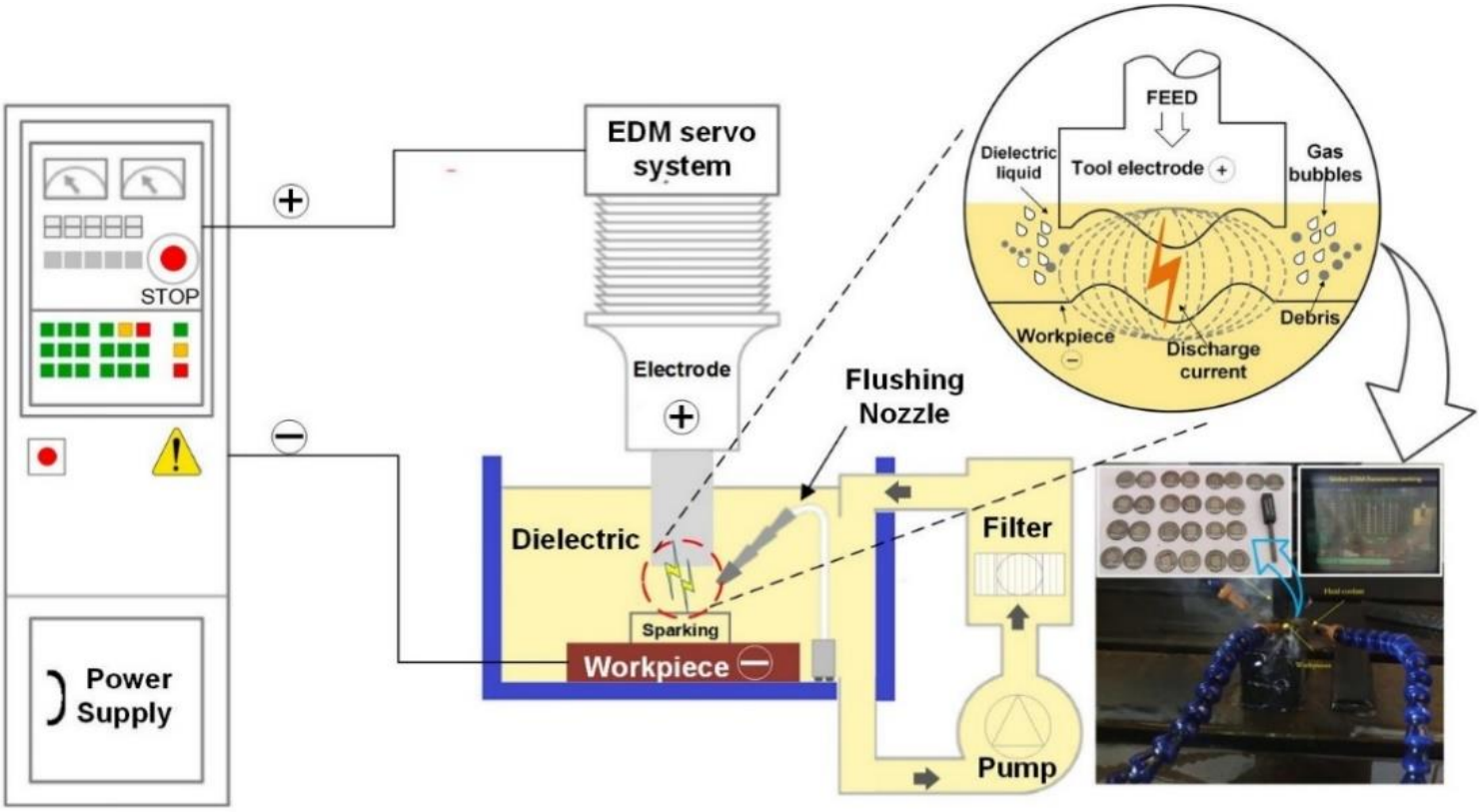

Fig. 3. Schematic Diagram of the SEDM Process using C-TEK ZNC™-50A

2.4. **ANOVA and statistic validation**

Analysis of variance (ANOVA) was used to determine the contribution of each parameter to the response [12, 17-20]. ANOVA compares the means of the three input variables to assess whether there are significant differences between them (Table 1). This analysis helps ascertain whether data variations are attributed to different treatments (factors) or random variability [21-24].

Table 1. SEDM Parameters

Run	SEDM Parameter		
	Pulse current, A	Gap voltage, V	Spark on time, (µs)
1	16	50	305
2	13	40	210
3	10	45	210
4	10	40	305
5	10	50	305
6	13	50	210
7	10	45	400
8	16	45	210
9	16	45	400
10	13	50	400
11	13	40	400
12	13	45	305
13	16	40	305

Generally, ANOVA is based on the p-value, which indicates the likelihood that the observed differences between group means occur by chance. If the p-value was less than the predetermined significance level (typically 0.05), we concluded that there was a significant difference between the groups. Additionally, ANOVA can assess the contribution of each parameter based on the Adjusted Sum of Squares (Adj SS) of each input parameter relative to the total Adj SS of all input parameters.[24-26].The Adjusted Sum of Squares provides insight into how much of the total variation in the data can be explained by each tested factor. By comparing the Adj SS of each parameter with the total Adj SS, we can identify the parameters that contribute most significantly to the variation in the results.

3. Result and discussion

3.1. **Surface profile, Ra**

The surface profile (*Ra*) data from the samples were measured using an Elcometer™ and are summarized in Table 2. The results show that the smoothest surface profile was obtained in iteration number 2, followed closely by iteration number 13, with average surface profiles of 8.55 microns and 9.50 microns, respectively. For iteration number 2, the settings included a pulse current of 13 A, gap voltage of 40 V, and spark time of 210 µs. In contrast, iteration number 13 utilized a pulse current of 16 A, gap voltage of 40 V, and spark-on time of 305 µs.

A statistical analysis was conducted on *Ra* to establish a correlation equation incorporating the three variables that influence *Ra*. The resulting correlation equation, derived through linear regression, is given by Eq. (1). Where A, B, and C are the pulse current, gap voltage (V), and spark-on time (µs), respectively.

$$Ra=4.76-0.145*A+0.1187*B + 0.00897* C \quad (1)$$

The Ra characterization for iterations 2 and 13 was conducted using a digital camera, with an analysis based on the *Ra* values determined through color intensity, monochrome, and binary representations, as shown in Fig. 4. Analysis of the surface images, arranged in three rows with varying Ra values (Ra), revealed significant differences in the distribution of *Ra*. In the first row, which uses a black-red color scale, it is clear that as the *Ra* value increases, the area covered by red also increases. This indicates that surfaces with higher *Ra* values (e.g., 10.4 µm) had a larger rough area than those with lower Ra values (8.3 µm). The expanded red region reflects a greater number of peaks and valleys on the surface, suggesting increased roughness.

The second row of Fig. 4 provides a monochrome view that enhances the visualization of the surface texture. Higher *Ra* values are associated with a more pronounced rough and random appearance, as shown by the more distinct gradients between light and dark areas.

Table 2. Surface profile of SEDM results

Iterations	Parameters			Surface profile, *Ra*			
	A	B	C	Ra-1	Ra-2	Average	Predicted
1	16	50	305	10.5	10.6	10.55	11.1
2	13	40	210	8.3	8.8	8.55	9.5
3	10	45	210	11.6	11.7	11.65	10.5
4	10	40	305	10.4	10.3	10.35	10.8
5	10	50	305	11.4	11.5	11.45	12.0
6	13	50	210	11.1	11.2	11.15	10.7
7	10	45	400	12.3	12.4	12.35	12.2
8	16	45	210	10.9	10.7	10.80	9.7
9	16	45	400	11.3	11.4	11.35	11.4
10	13	50	400	12.8	12.9	12.85	12.4
11	13	40	400	12.7	12.6	12.65	11.2
12	13	45	305	13.4	13.1	13.25	11.0
13	16	40	305	8.9	10.1	9.50	9.9

Surfaces with higher *Ra* values, such as 10.4 µm, exhibit more significant topographical variation and a more irregular texture distribution compared to those with lower *Ra* values.

The third row, which displays *Ra* in a black-and-white binary format, shows the differences between the peaks and valleys. The white areas indicate broader and more dispersed rough peaks at higher *Ra values.* The surface with *Ra* = 10.4 µm displays a more extensive white area and a more random distribution than the surface with *Ra* = 8.3 µm, which appears more uniform and smoother.

Overall, the three rows of images provide a detailed view of how *Ra* influences the surface texture and roughness distribution, with more significant variations corresponding to higher *Ra*. The first row uses a black-red color scheme to display surface roughness, showing *Ra* ranging from 8.3 µm to 10.4 µm, where the red areas indicate higher Ra_{ave} than others. The second row features a monochrome representation that enhances clarity; surfaces with lower *Ra* appear smoother, while the *Ra* = 10.4 µm surface exhibits more pronounced and irregular roughness patterns. The third row employs a binary (black-and-white) display to highlight the extreme roughness distribution, where surfaces with a higher *Ra* reveal more extensive white areas representing peaks or rough regions. The *Ra* = 10.4 µm shows a broader and more randomly distributed white area than the *Ra* = 8.3 µm surface.

This phenomenon aligns with the previous research reported by [10], which noted similar visualizations, as shown in Fig. 5. Fig. 5 shows the surface roughness in a monochrome format with Ra values ranging from 0.40 to 1.96. As shown in Fig. 4, an increase in *Ra* correlates with Ra_{ave} and a more irregular texture distribution. At a low *Ra* (0.40), the surface appears smoother, whereas at a high *Ra* (1.96), more areas exhibit sharp texture variations.

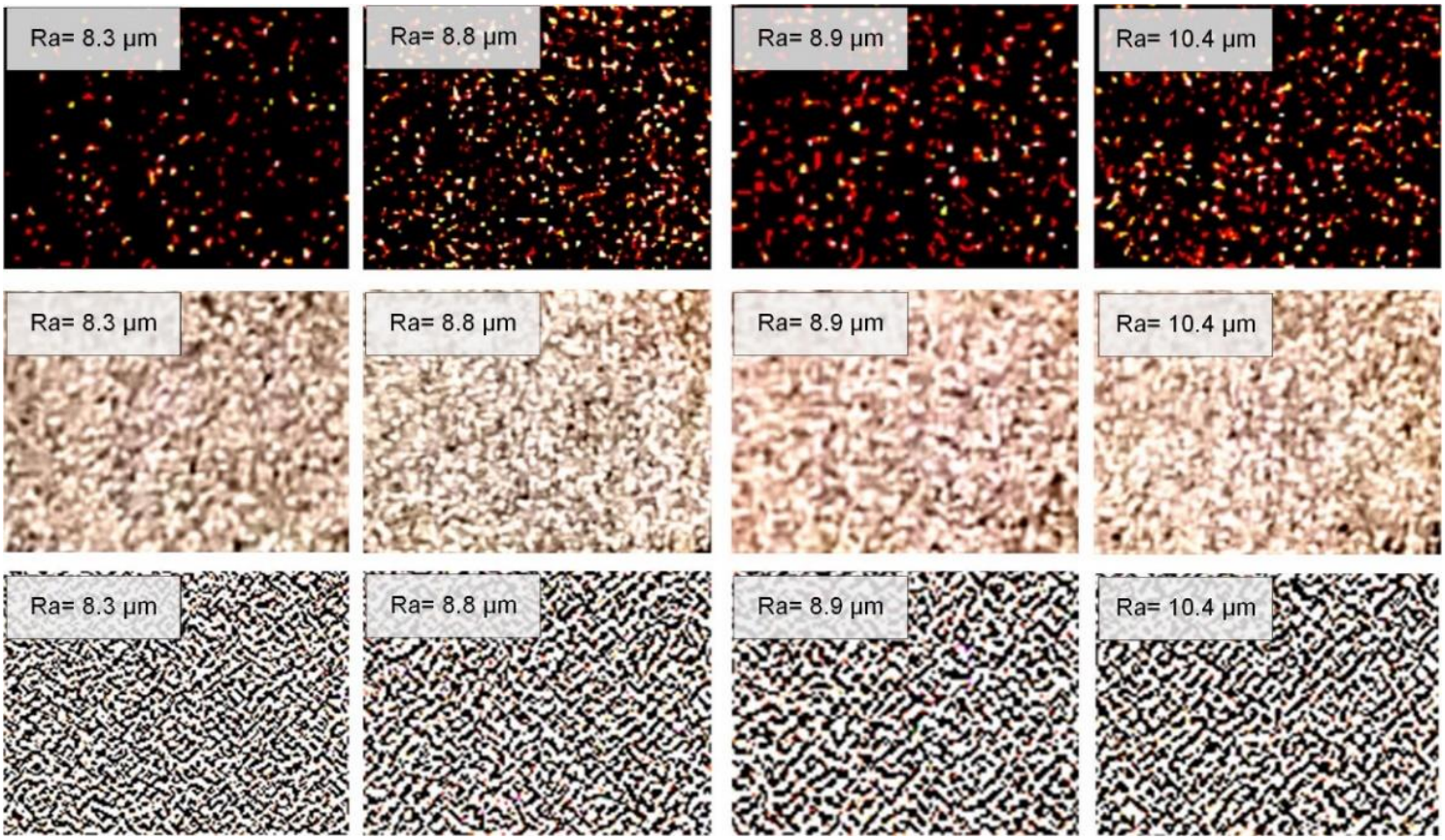

Fig. 4. Surface roughness characterization based on *Ra* values: color intensity representation (top row), monochrome (middle row), and binary (bottom row).

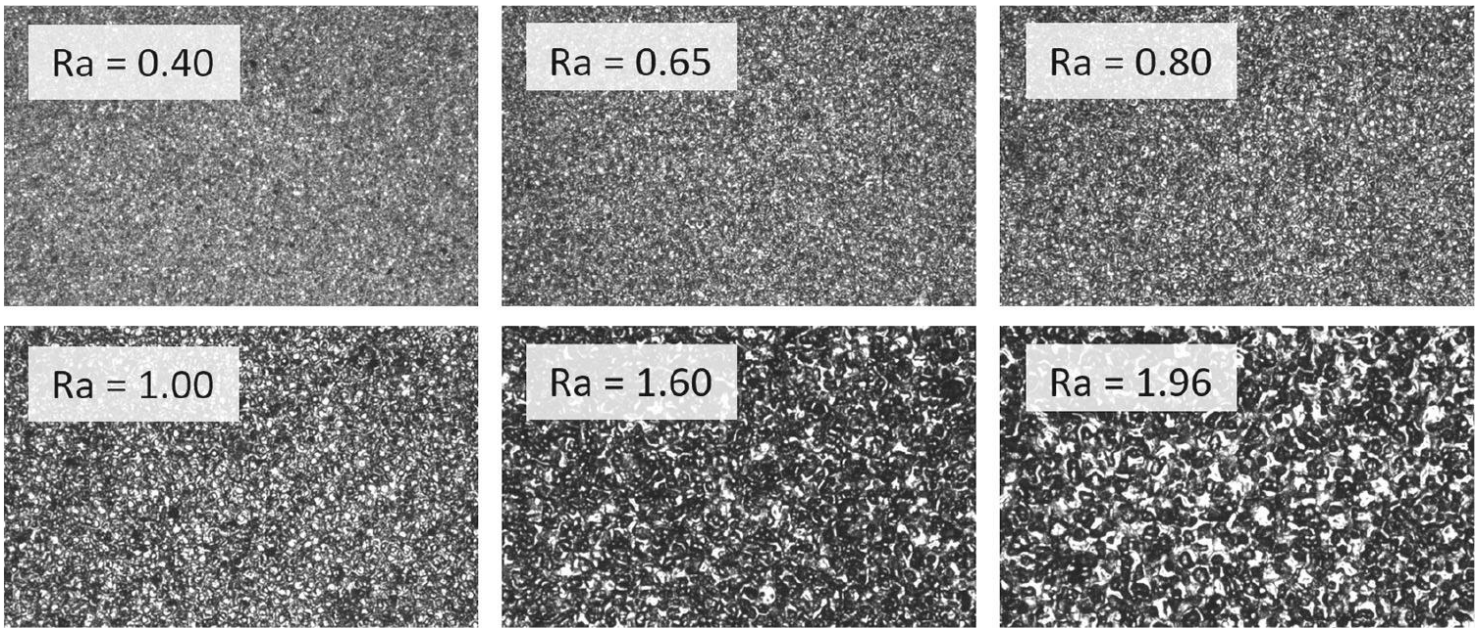

Fig. 5. The surface roughness characterization was adapted from a previous study [11]

Compared with Fig. 4, both images display a similar trend regarding the increase in surface roughness with higher Ra values. However, the visualizations in Fig. 4 are more complex, using three methods (color intensity, monochrome, and binary), which allows for a deeper analysis of the roughness distribution differences. Although Fig. 5 shows only a monochrome display, the results remain consistent, indicating that surfaces with higher *Ra* values have more peaks, increased profile areas, and fewer smooth regions.

In summary, this study confirms that a higher *Ra* correlates with increased surface roughness, as evidenced by both color and monochrome analyses. Both Fig.s clearly demonstrate that a higher *Ra* reflects a greater quantity of rough areas with a more random distribution and less uniform surface. The surface profiles in this study show an improvement of approximately 10% compared with the data reported by [11].

3.2. Surface plot analysis

Surface plot analysis is an essential part of the Response Surface Methodology (RSM) optimization approach. Based on the displayed surface plots of Ra-Ave, the optimal conditions for achieving the lowest surface roughness occurred for specific combinations of parameters A, B, and C, as shown in Fig. 6. In Fig. 6(a), it is evident that *the* Ra_{Ave} values decrease as A approaches 14-15 and B approaches 45-50, with C held constant at 305. This indicates that variations in A and B within this range have a significant impact on surface smoothing, providing a crucial foundation for further analysis.

Fig. 6(b) depicts the relationship between Ra and Ave and parameters B and C, with A set to 13. There was a decrease in Ra_{Ave} at B = 45 and C values between 200 and 300. This combination consistently reduced the surface roughness, suggesting that lower values of B and intermediate values of C created optimal conditions for surface processing.

Fig. 6(c) shows Ra_{Ave} against A and C with B fixed at 40. The findings indicate that combinations of A around 13-14 and C between 250-350 produce the smoothest surface. From these three plots, we can conclude that the optimal conditions are A = 14, B = 45, and C = 250-300, leading to the lowest surface roughness for the intended application. Among the three plots, plot (a) demonstrated the smoothest surface, as it had the lowest Ra_{Ave} compared to plots (b) and (c). In plot (a), with parameter combinations of A approximately 14-15 and B approximately 45-50, $Ra_{Ave.}$ reaches its minimum.

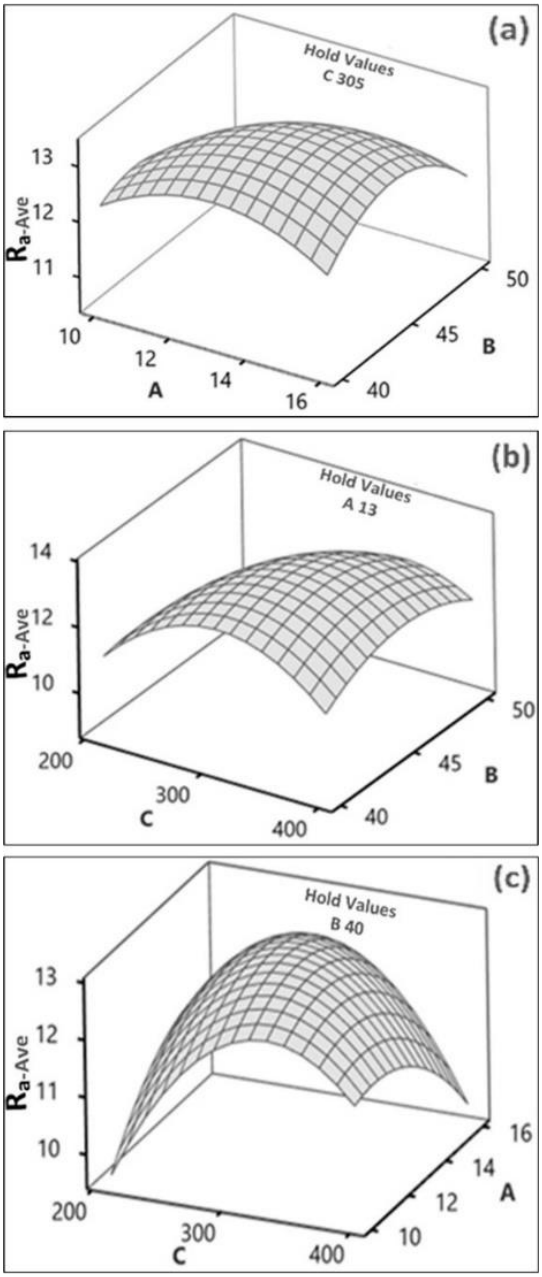

Fig. 6. Surface plot of surface profile: (a) $R_{a\text{-}Ave}$ vs A, B (b) Ra_{ave} vs B, C and (c) $R_{a\text{-}Ave}$ vs A, C

This indicates that the combination of A and B within this range yields a surface with lower roughness than those in the other plots, making it the most optimal choice.

3.3. ANOVA analysis

Analysis of variance (ANOVA) was performed using statistical software, resulting in 13 degrees of freedom. The analysis of the contributions focused solely on the effects of the three variables on the surface profile. Table 3 presents the ANOVA results. The results indicate that 'spark on time' (µs) is the variable that most significantly affects the response, followed by 'pulse current' and 'gap voltage,' with contributions of 13.26%, 27.66%, and 59.08%, respectively. These findings align with the previous research reported by [10], which noted that "Spark on Time" (µs) has a significant impact.

Table 3. ANOVA statistical and contributions

Parameters	Adj SS	F-Value	Contributions
A	0.9113	0.55	13.26%
B	1.9012	1.15	27.66 %
C	4.0613	2.45	59.08%

4. Conclusion

The analysis of the three surface plots indicates that optimal conditions for minimal Ra occur in plot (a), with A approximately at 14-15, B approximately at 45-50, and C at 305. Under these settings, Ra-Ave values were the lowest, confirming that A and B significantly affect surface smoothness. This suggests that variations in parameters A and B significantly influence the smoothness of the surface during the analysis process. Characterizing the surface roughness in iterations 2 and 13 using digital analysis revealed significant differences based on color intensity, monochrome, and binary displays. In the black-red display, the increase in *Ra* values (from 8.3 µm to 10.4 µm) results in a larger red area, reflecting higher roughness. The monochrome display clarifies the surface texture, where a higher *Ra* value indicates a rougher and more random surface. The black-and-white binary profile further highlighted the differences in roughness, with broader and more dispersed peaks at higher *Ra* values.

Acknowledgements

This research was fully funded by the Ministry of Education and Culture through the Novice Lecturer Research Program under contract number 106/E5/PG.02.00.PL/2024 (June 11, 2024) and 106/SP2H/RT-MONO/LL4/2024 (June 14, 2024). Special thanks to all parties who contributed to this research, enabling the collection of comprehensive data.

References

[1] U. Ashok Kumar and P. Laxminarayana, "Optimization of Electrode Tool Wear in micro holes machining by Die Sinker EDM using Taguchi Approach," Materials Today: Proceedings, vol. 5, no. 1, pp. 1824-1831, 2018.

[2] A. Moghanizadeh, "Reducing side overcut in EDM process by changing electrical field between tool and work piece," International Journal of Advanced Manufacturing Technology, vol. 90, no. 1-4, pp. 1035-1042, 2017.

[3] C. C. Wang and B. H. Yan, "Blind-hole drilling of Al2O3/6061Al composite using rotary electro-discharge machining," 2000, vol. 102, pp. 90-102.

[4] P. Balasubramanian and T. Senthilvelan, "Optimization of Machining Parameters in EDM Process Using Cast and Sintered Copper Electrodes," Procedia Materials Science, vol. 6, no. Icmpc, pp. 1292-1302, 2014.

[5] N. V. Kousik, N. Yuvaraj, R. Arshath Raja, P. Palanivel, and N. V. Kousik, "EDM Process by Using Copper Electrode with INCONEL 625 Material," IOP Conference Series: Materials Science and Engineering, vol. 811, no. 1, 2020.

[6] N. M. Elsiti, M. Y. Noordin, and A. U. Alkali, "Fabrication of high aspect ratio micro electrode by using EDM," IOP Conference Series: Materials Science and Engineering, vol. 114, no. 1, 2016.

[7] E. Aliakbari and H. Baseri, "Optimization of machining parameters in rotary EDM process by using the Taguchi method," International Journal of Advanced Manufacturing Technology, vol. 62, no. 9-12, pp. 1041-1053, 2012.

[8] T. Sultan, A. Kumar, and R. D. Gupta, "Material Removal Rate, Electrode Wear Rate, and Surface Roughness Evaluation in Die Sinking EDM with Hollow Tool through Response Surface Methodology," International Journal of Manufacturing Engineering, vol. 2014, pp. 1-16, 2014.

[9] R. Swiercz, D. Oniszczuk-Swiercz, L. Dabrowski, and J. Zawora, "Optimization of machining parameters of electrical discharge machining tool steel 1.2713," AIP Conference Proceedings, vol. 2017, no. October, 2018.

[10] J. Saeedi et al., "Measurement and inspection of electrical discharge machined steel surfaces using deep neural networks," Machine Vision and Applications, vol. 32, no. 1, 2020.

[11] S. Sumanto et al., "Enhancement Material Removal Rate Optimization of Sinker EDM Process Parameters Using a Rectangular Graphite Electrode," Jurnal Optimasi Sistem Industri, vol. 21, no. 2, pp. 87-96, 2022.

[12] K. Khoirudin, S. Sukarman, N. Rahdiana, A. Suhara, and A. Fauzi, "Optimization of S-EDM Process Parameters on Material Removal Rate Using Copper Electrodes," Jurnal Polimesin, vol. 21, no. 1, pp. 17-20, 2023.

[13] Y. Jia, G. Chi, W. Li, Z. Wang, and L. Cui, "Influence of wear pattern of graphite electrode on EDM geometric accuracy of slot machining," Procedia CIRP, vol. 95, pp. 408-413, 2020.

[14] A. Muttamara, W. Borwornkiatkaew, A. Pronpijit, and S. Nuanchom, "Effect of Graphite Electrode to Surface's Characteristic of EDM," in MATEC Web of Conferences, 2016, vol. 70.

[15] JIS G 4404 Alloy Tool Steels, 2015.

[16] Siswanto et al., "Box-Behnken Response Surface Methodology: An Analysis of the Effect of Variations in TIG Welding Parameters on Tensile Strength and Hardness Using SUS 304 Material," Annales de Chimie - Science des Matériaux, vol. 48, no. 3, 2024.

[17] K. Khoirudin, S. Sukarman, N. Rahdiana, and A. Fauzi, "Analisis Fenomena Spring-Back/ Spring-Go Factor Pada Lembaran Baja Karbon Rendah Menggunakan Pendekatan Eksperimental," Jurnal Teknologi, vol. 14, no. 1, 2022.

[18] D. Mulyadi et al., "The Box-Behnken Response Surface Methodology Approach to Optimize Tensile Strength Load in Resistance Spot Welding Using SPCC-SD Steel," Jurnal Teknik Mesin Mechanical Xplore, vol. 4, no. 2, pp. 47-60, 2024.

[19] K. Khoirudin, S. Sukarman, S. Siswanto, N. Rahdiana, and A. Suhara, "Analysis of Spring-back and Spring-go on Variation of V-Dies Bending Angle Using Galvanized SGCC Steel Sheet," Jurnal Teknik Mesin Mechanical Xplore (JTMMX), vol. 3, no. 1, pp. 17-25, 2022.

[20] K. Khoirudin, M. Murtalim, S. Sukarman, R. H. Anwar, M. A. Rahman, and N. Rahdiana, "Penerapan Lemari Asap untuk Meningkatkan Hasil Produksi Telur Asin pada Kelompok Usaha Telur Bebek," 2021, pp. 1-6.

[21] P. Muthu, "Optimization of the Process Parameters of Resistance Spot Welding of AISI 316l Sheets Using Taguchi

Method," Mechanics and Mechanical Engineering, vol. 23, no. 1, pp. 64-69, 2019.
[22] A. K. Biradar and B. M. Dabade, "Optimization of resistance spot welding process parameters in dissimilar joint of MS and ASS 304 sheets," Materials Today: Proceedings, vol. 26, no. xxxx, pp. 1284-1288, 2019.
[23] A. Amar et al., "Enhancing TIG Welding Parameters For Direct Tensile Load (DT-load) On Various Steel Thicknesses," J u r n a l P o l i m e s i n, vol. 22, no. 1, pp. 112-119, 1 February 2024 2024.
[24] A. Budianto, S. Sukarman, S. B. Jumawan, and A. Abdulah, "Optimasi Respon Tunggal Pada Proses Texturing Benang DTY-150D / 96F Menggunakan Metode Taguchi Single Response Optimization oF DTY-150D / 96F Yarn Texturing Process Using Taguchi Method," Arena Tekstil, vol. 35, no. 2, pp. 77-86, 2020.
[25] Minitab. (2023, 10/12/2023). Overview for Probability Plot.
[26] P. G. Mathews, Design of Experiments with MINITAB, 12 ed. Milwaukee: Mathews, Paul G., 2005, pp. 205-205.